Observation of a Spin Gap in the Normal State of Superconducting Mo_3Sb_7

Vinh Hung Tran and Wojciech Miiller

W. Trzebiatowski Institute of Low Temperature and Structure Research, Polish Academy of Sciences, P.O. Box 1410, 50-950 Wrocław, Poland

Zbigniew Bukowski

Laboratory for Solid State Physics, ETH Zürich, 8093 Zürich, Switzerland

(Received 29 November 2007; published 1 April 2008)

Magnetization, specific heat, and electrical resistivity measurements have been performed on the superconductor Mo_3Sb_7. Two kinds of transitions are observed at 2.3 and 50 K, respectively. The former is superconducting transition, while the latter is attributed to spin-gap formation. From the analysis of the experimental data, excitation gap, intra- and interdimer interactions are estimated as $\Delta/k_b \sim 120$ K, $J_0/k_B \sim 150$ K, and $J_1/k_B \sim 55$ K. The electronic structure calculations using the LSDA approximation show nesting property in the Fermi surface, favoring the superconductivity.

DOI: 10.1103/PhysRevLett.100.137004 PACS numbers: 74.70.Ad, 74.25.Bt, 74.25.Ha, 74.78.−w

Low-dimensional (LD) correlated electronic systems (CES) are intensively studied due to the richness of the physical phenomena. Unusual superconducting states observed in layered cuprates [1], charge or spin density waves (CDW, SDW) in superconducting organic salts [bis-(tetramethyl-tetraselenafulvalene)hexafluorophosphate, or $(TMTSF)_2PF_6$] and $\kappa - (ET)_2Cu[N(CN)_2](Br, Cl)$, [2] and spin Peierls (SP) in inorganic compound $CuGeO_3$, [3] are typical examples of LD systems. It is now generally accepted that the interplay between the dimensionality of a given system and the symmetry of the order parameter determines ground states. However, they are very often in competition, for instance, there are mixed CDW and SDW states, and there is evidence for the coexistence of antiferromagnetism and superconductivity and also the appearence of superconductivity bekow the pseudogap. For these reasons, the physical properties of LD CES are still not well understood.

Some years ago, Bukowski *et al.* [4] reported the superconductivity in an intermetallic Mo_3Sb_7. The superconducting phase transition of this material has been determined from measurements of magnetization, electrical resistivity,[4] and point-contact (PC) Andreev-reflection,[5] on a single crystal to be 2.08 K. In recent work, Tran *et al.*, [6] have measured low-temperature specific heat on a polycrystalline sample and found a large Sommerfeld coefficient, which has been attributed to a narrow Mo 4*d* band pinned at the Fermi level. Furthermore, the electronic specific heat in the superconducting state has been ascribed to the presence of two BCS-like gaps with $2\Delta_1 = 4.0k_BT_c$ and $2\Delta_2 = 2.5k_BT_c$. Candolfi *et al.* [7] have reported magnetic susceptibility, specific heat, and electrical resistivity down to 0.6 K and have interpreted their data within the frameworks of the spin fluctuation theory. Here, we report another anomalous feature for Mo_3Sb_7 found in magnetic susceptibility, specific heat, and electrical resistivity measurements. It is anomaly appearing at 50 K, for which the behavior may be interpreted as the opening of a spin gap. Besides, the Mo_3Sb_7 compound has a unique crystal structure, which is built by three orthogonal alternating stacks of the magnetic Mo ions (-Mo-Mo-4Mo-Mo-Mo-), each sharing chain with sandwiched 4Sb prisms. Since, the distance Mo-Mo within the Mo-Mo pair (0.3 nm) is much shorter than those between Mo and 4Mo block (0.46 nm) or between chains (0.52 nm), one suspects that the intradimer interaction (e.g., within the Mo-Mo pair) is dominating. Such a LD character together with the gaplike feature of compound, the behavior of superconductor Mo_3Sb_7 resembles very much the case of LD CES mentioned above.

The investigated polycrystalline sample of Mo_3Sb_7 ($a = 0.9551$ nm) was prepared by an annealing process and was characterized by EDX and powder x-ray diffraction as described in detail in Ref. [6]. The magnetization was measured in a SQUID magnetometer (Quantum Design). The specific heat was measured using a thermal relaxation method, while the electrical resistivity was measured using ac technique, both utilizing PPMS platform (Quantum Design). Fermi surface of Mo_3Sb_7 was determined using the fully-relativistic version of the full-potential local-orbital minimum-basis band-structure scheme (FPLO) code [8]. In the calculations we used 816 irreducible *k* points.

Figure 1 displays the temperature dependence of the mole magnetic susceptibility $\chi_M(T) = M/\mu_0 H$ for Mo_3Sb_7. The bulk superconductivity of the compound is observed below 2.3 K as evidenced by the diamagnetic component found at low fields (not shown here). For magnetic fields up to 5 T, the Curie-Weiss type behavior of $\chi_M(T)$ is discernible at temperatures above 230 K. The best fit of the data yields an effective magnetic moment of 1.46(2) μ_B/Mo, somewhat smaller than the expected value for Mo ions with spin $S = 1/2$. A large paramagnetic Curie temperature of −970(30) K implies substantial antiferromagnetic interactions between Mo ions. The salient

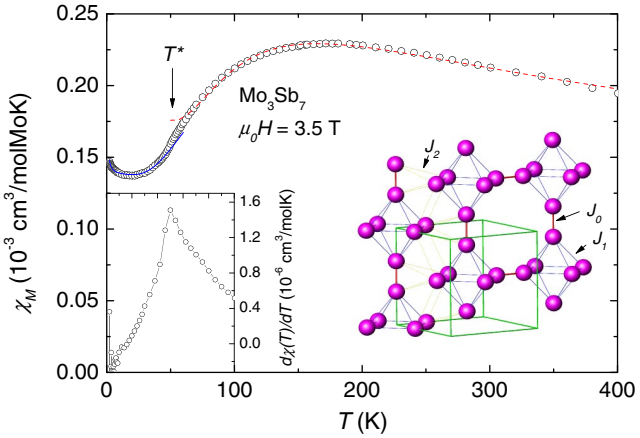

FIG. 1 (color online). Magnetic susceptibility of Mo_3Sb_7 measured at 3.5 T. The dashed and solid lines represent theoretical lines with the theoretical equations $\chi_{HT}(T)$ and $\chi_{LT}(T)$, respectively. The left-hand inset shows the temperature derivative of the magnetic susceptibility $d\chi(T)/dT$ and the right-hand inset schematic crystal structure of Mo_3Sb_7 with Mo ions as solid balls only. The intradimer J_0 and interdimer exchange interactions J_1 and J_2 are shown as thick and thin lines, respectively.

feature of the susceptibility is the appearance of a broad maximum around $T_{max} = 170$ K, which is one of the characteristic features of the low-dimensional systems [9,10]. The maximum in the $\chi(T)$-curve has also been observed by Candolfi *et al.* [7]. Considering the crystal structure of Mo_3Sb_7 (see right-hand inset of Fig. 1) we believe that the observed broad maximum in the susceptibility and the magnetic specific heat tail (see below) are associated with the short-range magnetic correlations due to the LD character of the studied compound. For isolated dimers, Bleaney and Bowers,[11] derived susceptibility equation based on the $S = 1/2$ Heisenberg Hamiltonian: $H = \sum_{i,j} JS_i.S_j$ as follows:

$$\chi_M = \frac{N_A \mu_B^2 g^2}{k_B T[3 + \exp(-2J_0/k_B T)]}, \quad (1)$$

where N_A is the Avogadro number, μ_B is the Bohr magneton, k_B is the Boltzmann constant and J_0 is the intradimer exchange coupling parameter. If taking into account the interdimer interaction $J' = 4J_1 + 8J_2$, the Eq. (1) becomes

$$\chi_M = \frac{N_A \mu_B^2 g^2}{k_B T(3 + \exp(-2J_0/k_B T) + J'/k_B T)}. \quad (2)$$

Fitting the experimental susceptibility data of Mo_3Sb_7 in the temperature range 60–400 K to the equation: $\chi_{HT}(T) = (1 - x)\chi_M(T) + \chi_0 + x0.375/T$, we get $x = 0.0085$, $\chi_0 = 0.1 \times 10^{-3}$ cm^3/(mol Mo) and $J_0/k_B = -152(5)$ K, $J'/k_B = 720(20)$ K. Assuming that the magnitude of the interdimer interactions is proportional to their corresponding distances, we may approach $J_2 \sim 1.13J_1$ and then one estimates J_1/k_B to be 55.4 K. These results suggest that Mo_3Sb_7 has a considerably stronger intradimer interaction compared to the interdimer one.

It should be noted that below $T^* = 50$ K the susceptibility drops sharply, causing a distinct maximum in the temperature derivative of the susceptibility (left-hand inset). We wish to add that the position of T^* is field independent for $\mu_0 H < 6$ T. We tentatively interpret the anomaly at $T^* = 50$ K as due to the opening of a gap in the spin excitation spectrum. Such a situation may be happen in Mo_3Sb_7 since coupling within Mo-Mo pairs tends to form a singlet state associated with the Mo-Mo ions dimerization. If such a gap scenario takes place in Mo_3Sb_7, the susceptibility below a characteristic temperature T^* may follow a gap function [12]:

$$\chi_{SG}(T) = b \exp(-\Delta_\chi/k_B T), \quad (3)$$

where b is a constant. The solid line in Fig. 1 is the best fit of the data to $\chi_{LT}(T) = \chi_0 + \chi_{CW}(T) + \chi_{SG}(T)$ with $\chi_0 = 0.14 \times 10^{-3}$ cm^3/mol, $\chi_{CW} = 7.08 \times 10^{-6}/T$ cm^3/(mol Mo), $b = 0.3 \times 10^{-3}$ cm^3/(mol Mo), and $\Delta_\chi/k_B = 145(10)$ K.

The most important finding in Fig. 2 is the appearance of a maximum in the specific heat $C_p(T)/T$ curve at the same temperature of $T^* = 50$ K, where the susceptibility drops suddenly. Thus, our $\chi(T)$ and $C_p(T)$ data differ from that of those reported by Candolfi *et al.* [7], who did not observe any anomaly around 50 K. To analyze the C_p data we assumed C_p to be the sum of three common components: the electronic, magnetic, and phonon ones. The electronic specific heat was deduced from the low-temperature data from the fit to the equation $C_p = \gamma T + \beta T^3$. In the temperature range 2.5–6 K we obtained $\gamma = 11.2$ mJ/(mol Mo)K^2 and $\beta = 0.283$ mJ/(mol Mo)K^4. The phonon specific heat C_{ph} of Mo_3Sb_7 is taken as the

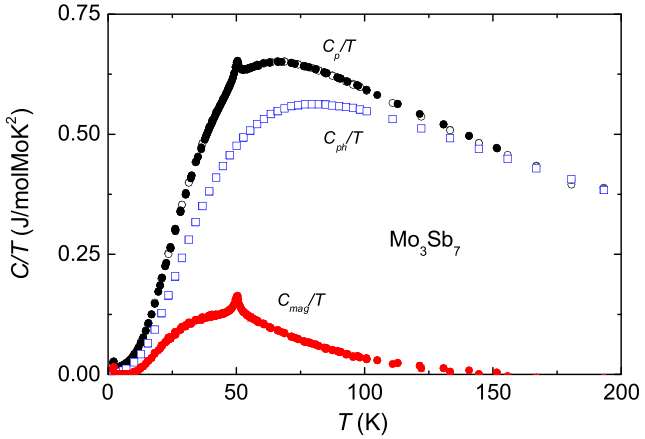

FIG. 2 (color online). The specific heat of Mo_3Sb_7 divided by temperature as a function of temperature. The phonon specific heat was calculated from the phonon part of specific heat of $Ir_3Ga_3Ge_4$ after correction of the mass effect. The magnetic specific heat is the difference $C_{mag} = C_{p,Mo_3Sb_7} - \gamma T - C_{ph}$.

lattice contribution to the specific heat of the isostructural compound $Ir_3Ga_3Ge_4$ exhibiting a weak diamagnetism [13]. Because the Debye temperature is inverse to the atomic mass m as $\Theta_D \sim 1/\sqrt{m}$, we may correct the mass effect on the specific heat of $Ir_3Ga_3Ge_4$ by a scaling $T_s = \sqrt{(m_{Ir_3Ga_3Ge_4})/(m_{Mo_3Sb_7})}T$, and as a result $C_{ph}(T) = \Delta C_{Ir_3Ga_4Ge_4}(T_s)$, where $\Delta C_{Ir_3Ga_4Ge_4}(T) = C_{p,Ir_3Ga_4Ge_4} - \gamma_{Ir_3Ga_4Ge_4}T$.

The magnetic specific heat, obtained from the difference $C_{mag} = C_p - \gamma T - C_{ph}$ is displayed in Fig. 3. Temperature dependence of the magnetic specific heat. For isolated dimers the magnetic specific heat has the following formula: [14,15]

$$C_D \sim \frac{(\Delta/k_BT)^2 \exp(\Delta/k_BT)}{[1 + 3\exp(\Delta/k_BT)]^2}. \quad (4)$$

In the low-temperature limit, the magnetic specific heat can be reduced to

$$C_D \sim (\Delta/k_BT)^2 \exp(\Delta/k_BT). \quad (5)$$

We have fitted the magnetic specific heat data in the temperature range 3–35 K to Eq. (5) with $\Delta/k_B = 113(5)$ K. The result of the fit shown as solid line in Fig. 3 reproduces the experimental data rather well. The observed value $\Delta_{Cp}/k_B = 113$ K is the same order of magnitude as deduced from the magnetic data ($\Delta_\chi/k_B = 145$ K), therefore providing a support for the gap opening. Bearing in mind the effect of the short-range (SR) interactions, manifested by the susceptibility maximum, we may examine the influence of the SR interactions on the specific heat. Taking $J/k_B = 152$ K from the magnetic data and using Eq. (4) we simulate the theoretical curve (dashed line). Thus, the bump around 55 K and the large tail in the $C_{mag}(T)$ above T^* may be ascribed to LD SR magnetic correlations.

To extract the magnetic entropy we have integrated the $S = \int_0^T \frac{C_{mag}/T'}{T'} dT'$. A rather small amount of entropy librated at T^* suggests that ascribing C_p peak at 50 K to any long-range Néel-type transition is questioned. Nevertheless, neutron diffraction and muon spin relaxation experiments are underway to determine eventual short-range spin ordering or a kink of hidden magnetism. Thus, at this stage we persist with interpretation in terms of spin-gap phenomenon for the anomaly in the $C_p(T)$ curve at 50 K and the exponential dependence of the $C_{mag}(T)$ curve. The lacking of peak in the temperature dependence of the susceptibility is consistent with this interpretation.

Figure 4 shows the temperature dependence of the electrical resistivity obtained by the four-probe method with the ac current strength of 5 mA and frequency of 47 Hz. As can be seen from the inset, the resistivity below 45 K varies as $\rho(T) = \rho_0 + cT + d\exp(-\Delta_\rho/k_BT)$, with $\rho_0 = 95.6 \times 10^{-8}$ Ωm, $c = 0.022 \times 10^{-8}$ Ωm/K, $d = 75 \times 10^{-8}$ Ωm, and $\Delta_\rho/k_B = 110(2)$ K. An attempt to fit the resistivity data with either T^2 or T^5 dependence produced worse agreement in the fit. Therefore, as in the case of the magnetic susceptibility and specific heat the behavior of the resistivity points to gap feature rather than to spin fluctuations. It should be mentioned that the sign of the pseudogap opening in superconducting cuprates is indicated in resistivity by the deviation downward from a temperature linear behavior [16–18]. For Mo_3Sb_7 the change in the slope of the $\rho(T)$-curve occurs around 50–60 K, and above 60 K linear T dependence of the resistivity is observed (thin line in Fig. 4).

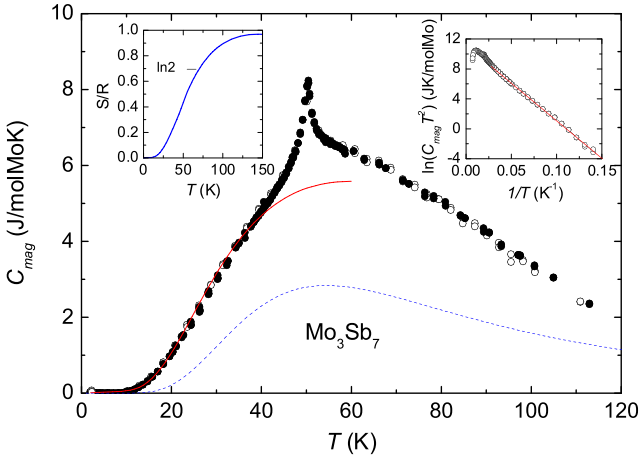

FIG. 3 (color online). Temperature dependence of the magnetic specific heat from two series of measurements. The solid and dashed lines show the theoretical values. The left hand inset shows magnetic entropy vs temperature. The right-hand inset shows the fit (solid line) of isolated dimer model in a full-gap state.

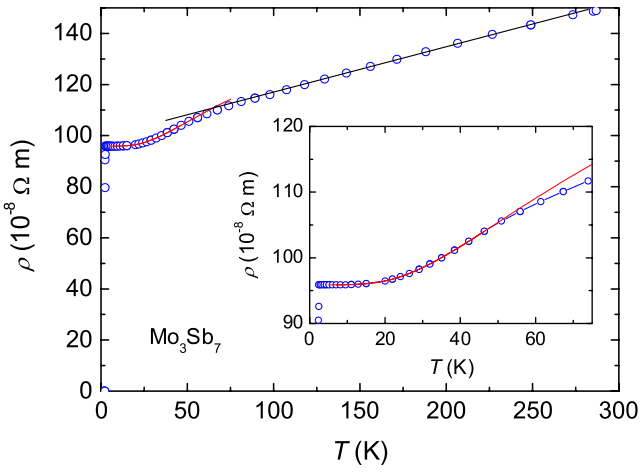

FIG. 4 (color online). Temperature dependence of the electrical resistivity. The thick and thin lines are theoretical. The inset shows the fit of low-temperature resistivity data to a gapped function.

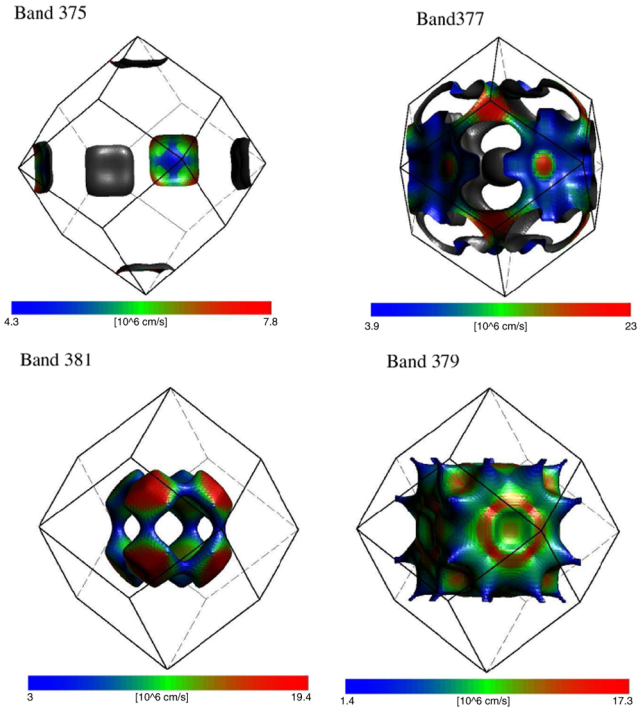

FIG. 5 (color online). Perfective view of the Fermi surfaces derived from the 375, 377, 379, and 381 bands of Mo_3Sb_7.

Figure 5 displays the theoretical Fermi surfaces for Mo_3Sb_7. The surfaces are presented with different colors, corresponding to different Fermi velocities. The hotter colors (orange and red) represent the Fermi regions of high Fermi velocities, while the colder colors (green and blue) the regions of low Fermi velocities. For Mo_3Sb_7, there are practically four bands denoted as 375, 377, 379, and 381,which have contributions to the Fermi surfaces. Looking from the figure, we see that the 375 band displays a stronger nesting compared to a greater dispersion in the 377 band. Obviously, the difference in Fermi velocities makes explicit the difference in quasiparticle bahavior in the ''hot'' and ''cold'' Fermi surface regions. Such a nesting property in the Fermi surface can favor for superconductivity.

In conclusion, we have shown that spins of the Mo^{5+} ions in the three-dimensional cubic system of Mo_3Sb_7 most probably evolve into a singlet state dimers, what cause a spin gap below 50 K, accompanied by anomalies in the magnetic susceptibility, specific heat, and resistivity. From the analysis of the experimental data the average excitation gap is evaluated to be about 120 K. We may suggest that even with the presence of a spin gap, the superconductivity can occur owing to the Fermi surface nesting. Finally, it is interesting that despite the difference in the critical temperatures of Mo_3Sb_7 and high-temperature superconductors we suppose that important features shared for superconductivity seem to be the appearance of a gap or pseudogap at temperature much higher than T_c. The issue of forming of eventual preformed BCS pairs in Mo_3Sb_7 whether there is any relationship between T^* and T_c in this compound should be clarified in the future studies.

The work at ILT& SR is supported by the Grant No. N202 082 31/0449 of the Ministry of Science and Higher Education in Poland.

[1] Z. Hiroi, M. Takano, M. Azuma, and Y. Takeda, Nature (London) **364**, 315 (1993).
[2] C. Bourbonnais and D. Jérome, *Advance in Synthetic Metals*, edited by P. Bernier, S. Lefrant, and G. Bedan (Elsevier, Amsterdam, 1999), p. 26.
[3] M. Hase, I. Terasaki, and K. Uchinokura, Phys. Rev. Lett. **70**, 3651 (1993).
[4] Z. Bukowski, D. Badurski, A. J. Stępień-Damm, and R. Troć, Solid State Commun. **123**, 283 (2002).
[5] V. M. Dmitriev, L. F. Rybaltchenko, L. A. Ishchenko, E. V. Khristenko, Z. Bukowski, and R. Troć, Supercond. Sci. Technol. **19**, 573 (2006); V. M. Dmitriev, L. F. Rybaltchenko, E. V. Khristenko, L. A. Ishchenko, Z. Bukowski, and R. Troć, Fiz. Nizk. Temp. **33**, 399 (2007).
[6] V. H. Tran and Z. Bukowski, arXiv: 0803.2948.
[7] C. Candolfi, B. Lenoir, A. Dauscher, C. Bellouard, J. Hejtmanek, E. Santava, and J. Tobola, Phys. Rev. Lett. **99**, 037006 (2007).
[8] K. Koepernik and H. Eschrig, Phys. Rev. B **59**, 1743 (1999).
[9] M. E. Fisher, J. Math. Phys. (N.Y.) **4**, 124 (1963).
[10] J. C. Bonner and M. E. Fisher, Phys. Rev. **135**, A640 (1964).
[11] D. Bleaney and K. D. Bowers, Proc. R. Soc. A **214**, 451 (1952).
[12] L. N. Bulaevskii, Sov. Phys. Solid State **11**, 921 (1969).
[13] V. H. Tran and Z. Bukowski (private communication). $Ir_3Ga_3Ge_4$ crystallizes in the cubic Ir_3Ge_7-type structure with the lattice parameter of $a = 0.8687$ nm. The magnetic measurements indicate a weak diamagnetism. The electronic specific heat coefficient γ was determined from the low-temperature data to be 3.5 mJ/(mol Ir)K^2. The phonon specific heat has two ingredients: Debye component $C_{\mathrm{ph},D}$ with the Debye temperature $\Theta_D = 275(5)$ K and Einstein component $C_{\mathrm{ph},E}$ with the Einstein temperature $\Theta_E = 110$ K.
[14] R. L. Carlin, *Magnetochemistry* (Springer-Verlag, Berlin, 1986).
[15] H. Kageyama, K. Onizuka, Y. Ueda, M. Nohara, H. Suzuki, and H. Takagi, J. Exp. Theor. Phys. **90**, 129 (2000).
[16] B. Bucher, P. Steiner, J. Karpinski, E. Kaldis, and P. Wachter, Phys. Rev. Lett. **70**, 2012 (1993).
[17] M. Oda, K. Hoya, R. Kubota, C. Manabe, N. Momono, T. Nakano, and M. Ido, Physica (Amsterdam) **281C**, 135 (1997).
[18] Y. Abe, K. Segawa, and Y. Ando, Phys. Rev. B **60**, R15 055 (1999).